Migration of Cytotoxic T Lymphocytes in 3D Collagen Matrices

Z. Sadjadi*, R. Zhao, M. Hoth, B. Qu, and H. Rieger

To fulfill their killing functions, cytotoxic T lymphocytes (CTLs) need to migrate to search for their target cells in complex biological microenvironments, a key component of which is extracellular matrix (ECM). The mechanisms underlying CTL's navigation are not well understood so far. Here we use a collagen assay as a model for the ECM and analyze the migration trajectories of primary human CTLs in collagen matrices with different concentrations. We observe different migration patterns for individual T cells. Three different motility types can be distinguished: slow, fast and mixed motilities. Slow CTLs remain nearly stationary within the collagen matrix and show slightly anti-persistent motility, while the fast ones move quickly and persistent (i.e. with not too large turning angles). The dynamics of the mixed type consists of periods of slow and fast motions; both states are persistent, but they have different persistencies. The dynamics can be well described by a two-state persistent random walk model. We extract the parameters of the model by analyzing experimental data. The mean square displacements predicted by the model and those measured experimentally are in very good agreement, without any fitting parameter. Potential reasons for the observed two-state motility are discussed. T cells dig the collagen during their migration and form channels, which facilitate the movement of other CTLs in the collagen network.

I. INTRODUCTION

Cytotoxic T lymphocytes (CTLs) are fully activated $CD8^+$ T cells, which are key players in the adaptive immune system to eliminate tumorigenic or pathogen-infected cells [1]. CTLs need to find their cognate antigens or cancerous cells, which are low in number[2, 3]. Thus, the ability of CTLs to efficiently navigate and search is crucial for an efficient immune response. Migration behavior of immune cells in the body and the search strategies they might follow is currently of great interest in physics and biology[4–6]. Migration of naive T cells in lymph nodes reportedly follows a Brownian or even subdiffusive dynamics [7–9], but switchings between fast and slow motility modes have been also observed [10]. Outside the lymph node, activated T cells destined to find their targets in peripheral tissues, most of which are characterized by dense extracellular matrix (ECM) [11]. Here a faster migration, e.g. via longer phases of superdiffusive dynamics or less switchings to the slow diffusive mode, is advantageous to be able to scan a larger tissue efficiently. For instance, it was reported that the dynamics of $CD8^+$ T cells in infected brain tissue resembles a Levy walk [12].

The extracellular matrix (ECM) mainly consists of collagens and is the major component of all tissues and organs. It has essential regulatory roles in nearly all cellular functions. Some collagens have inhibitory effects on the function of different immune cells [13, 14]. In various types of cancer, the collagen network becomes dense, stiff and linearized in the vicinity of tumors, facilitating the transport of cancerous cells and making the ECM an important player in cancer metastasis, intravasion and prognosis [15–20]. Additionally, the activity of T cells is also influenced by the density of the collagen matrix in tumors [21]. Recently, different immune cells have been investigated in immunotherapy studies as potential drug delivery vehicles into the tumors [22, 23]. Understanding the migration and interactions of immune cells in collagen networks is crucial to unravel the underlying details of the immune response and design effective treatment strategies.

Collagen-based assays have been used to investigate the migration of lymphocytes in ECM and study the possible underlying mechanisms of immune interactions with ECM [13, 24–28]. In a recent study, collagen hydrogels were employed to compare migration patterns of human $CD8^+$ T cells in aligned and nonaligned collagen fibers as microenvironments resembling tumor cells and normal tissues, respectively [29].

In this study, we use bovine collagen to construct a 3D environment in vitro as a model for the ECM. The trajectories of primary human CTLs in collagen matrices with different concentrations are analyzed for two blood donors. We find three different types of motion in both donors: The migration of CTLs can be categorized into slow, fast and mixed sub-groups. In the latter case, T cells switch between two persistent states with different persistencies. Such two-state motilities may point toward the possible involvement of search optimization processes [30]. We employ a stochastic random walk model developed for active processes with two arbitrary states [31] to describe the trajectories of of T cells migrating in collagen. By extracting the model parameters from experimental data, we analytically reproduce the MSD results obtained from experiments, remarkably without any free parameter.

II. MATERIALS AND METHODS

Ethical considerations: Research carried out for this study with human material (leukocyte reduction system chambers from humanblood donors) is authorized by the local ethic committee (decleration from 16.4.2015 (84/15; Prof. Dr. Rettig-Stürmer)).

Human primary cytotoxic T lymphocytes (CTL) isolation, stimulation and nucleofection of CTLs: Peripheral blood mononuclear cells (PBMC) were obtained from

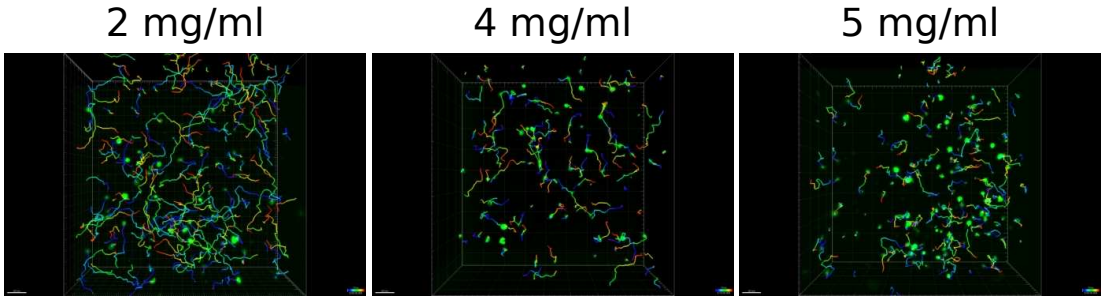

FIG. 1. CTL migration trajectories measured by lightsheet microscopy in in three dimensional collagen matrices with different concentrations. The nuclei of human primary CTLs are labeled with overexpressed Histone 2B-GFP (green). CTL migration trajectories are tracked automatically using Imaris. Scale bars are 40 μm.

healthy donors as previously described [32]. Human primary CTLs were negatively isolated from PBMC using Dynabeads^{TM} Untouched^{TM} Human CD8 T Cells Kit (ThermoFisher Scientific) or CD8$^+$ T Cell Isolation Kit, human (Miltenyi Biotec), stimulated with Dynabeads^{TM} Human T-Activator CD3/CD28 (ThermoFisher Scientific) in AIMV medium (ThermoFisher Scientific) with 10% FCS and 33 U/mL of recombinant human IL-2 (ThermoFisher Scientific). 48 hours after stimulation beads were removed and 5×10^6 CTLs were electroporated with 2 μg plasmid (H2B-GFP to label nucleus [33] or pMax-mCherry to label cell body) using the Human T cell nucleofector kit (Lonza). Medium was changed 6h after nucleofection and transfected CTLs were maintained in AIMV medium (ThermoFisher Scientific) with 10% FCS and 33 U/mL of recombinant human IL-2 (ThermoFisher Scientific). Cells were used 24-36 hours after nucleofection [34].

3D live cell imaging with lightsheet microscopy

3D live cell imaging using lightsheet microscopy was conducted mainly as described previously [35]. Briefly, human primary CTLs were resuspended first in PBS (ThermoFisher Scientific), afterwards neutralized collagen stock solution (bovine collagen type I, 8 mg/mL, Advanced Biomatrix) was added to a final concentration of 2 mg/ml, 4 mg/ml, or 5 mg/ml collagen with a cell density of 10×10^6 cells/ml. 20 μl of this cell/collagen mixture was loaded in a capillary. The capillary was closed and incubated for 60 min in an incubator. Afterwards, the polymerized collagen rod was pushed out hanging in the medium at $37C$ with 5% CO_2 for equilibration for another 60 min. To visualize collagen structure, analyzed collagen matrix was stained with 50 μg/ml Atto 488 NHS ester (ThermoFisher Scientific) in AIMV medium at room temperature after collagen polymerization. Afterwards, matrix was washed in AIMV medium. After collagen polymerization, cells in matrix with or without collagen staining were incubated in AIMV medium with 10% FCS at $37°C$ with 5% CO_2 for 1 hour. Afterwards, the migration of cells was visualized by lightsheet microscopy (20×objective) at $37°C$ with a z-step size of 1 μm and time interval of 30 seconds. The CTLs were transiently transfected with histone 2B-GFP or mCherry. The migration trajectories were tracked and analyzed using Imaris 8.1.2 (containing Imaris, ImarisTrack, ImarisMeasurementPro, ImarisVantage; Bitplane AG, software available at http://bitplane.com) [35].

III. EXPERIMENTAL RESULTS

To investigate migration patterns of CTLs in a 3D environment, we embedded primary human CTLs into collagen matrices and visualized their movements using lightsheet microscopy (Fig. 1). Different concentrations of collagen mimic the ECM of normal tissue (2 mg/ml), soft solid tumor (4 mg/ml) and hard solid tumor (5 mg/ml), respectively[36–38]. The experimental trajectories consist of a set of T cell positions recorded after equal time intervals. Every two successive recorded positions are used to calculate the instantaneous velocity, and every three of them to extract the corresponding turning angle ϕ. The instantaneous persistency can be defined as $\mathcal{R}_n = \cos\phi$. The global persistency $\mathcal{R}$ is the average over all $\mathcal{R}_n$s. The resulting parameters are summarized in Table I. The average velocity is higher at lower densities of collagen as expected, but the persistency of T cells is independent of the collagen concentration. The cross correlation between velocity and persistency, $CC_{v,\mathcal{R}} = (\langle v\mathcal{R}\rangle - \langle v\rangle\langle\mathcal{R}\rangle)/\sigma_v\sigma_{\mathcal{R}}$, which shows how these two parameters are related, also shows no systematic dependence on the collagen density. This value is in all cases positive, indicating that faster T cells move more persistent then slow ones. The distributions of velocity, turning-angle and persistency are shown in Fig. 2. The distributions of $\mathcal{R}_n$ and ϕ show an overall persistent random walk for all data sets by a tendency to turn with an angle around 0.4 to 0.5 radian (corresponding to a persistency around $\mathcal{R}\simeq 0.9$). This angle could reflect the structure of the collagen network.

Mean square displacement. To better understand the dynamics of T cells in different donors and collagen con-

TABLE I. Key statistical parameters of T cells in collagen matrices with different densities.

	Donor 1			Donor 2		
density ($\frac{mg}{ml}$)	2	4	5	2	4	5
velocity ($\frac{\mu m}{s}$)	0.10± 0.04	0.06± 0.03	0.05± 0.05	0.07± 0.03	0.04± 0.02	0.03± 0.01
persistency $\mathcal{R}$	0.30± 0.30	0.36± 0.29	0.35± 0.29	0.30± 0.30	0.36± 0.30	0.44± 0.25
$CC_{v,\mathcal{R}}$	0.64	0.35	0.35	0.36	0.29	0.31

centrations we analyze the mean square displacement (MSD) separately for each experimental condition. Figure 3 shows the MSD of two donors in different collagen concentrations. In all cases an initial diffusion or sub-diffusion is followed by a slight supper-diffusive motion. Eventually a crossover to diffusion is observed which is expected because on longer time scales the trajectories are randomized and the orientational memory is lost.

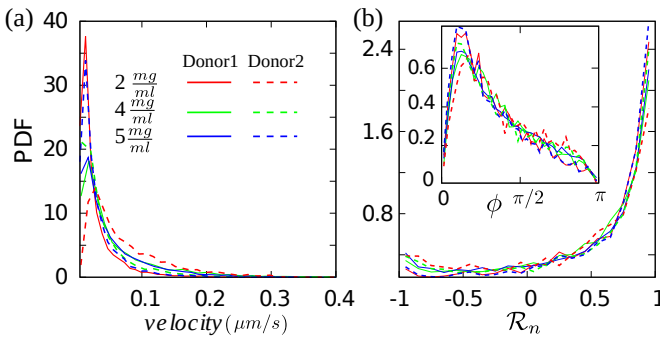

FIG. 2. Distributions of (a) velocity, and (b) persitency of T cells in collagen networks with different concentrations. Turning-angle distributions are shown in the inset.

A. Three motility groups can be distinguished in CTL dynamics.

Single track analysis of CTL trajectories reveals that there are three different types of CTL trajectories: (i) slow T cells which perform a sub-diffusive motion and their velocities always remain below a threshold value, (ii) a faster group with velocities always above a threshold value, and (iii) the third group with velocities which switch between fast and slow modes. Both donors have CTL of these three types, though with different proportions of them (shown in Table II). The velocity evolution of typical tracks of T cells and a few trajectories for each cell motility type are shown in Fig. 4.

We consider two velocity thresholds to distinguish the three types. All T cells whose maximum (minimum) velocity is less (more) than v_{c1} (v_{c2}) are categorized as slow (fast) type. Trajectories with $v_{max} > v_{c2}$ and $v_{min} < v_{c1}$ lie in the mixed category. Around 6 to 8 percent of T cells belong to non of these groups with varying parameters v_{c1} and v_{c2}. Figures 5(a,b) summarize the average velocities and persistencies of different types in different collagen concentrations for both donors. A slight overal increase (decrease) in the persistency (velocity) is observed with increasing collagen concentration.

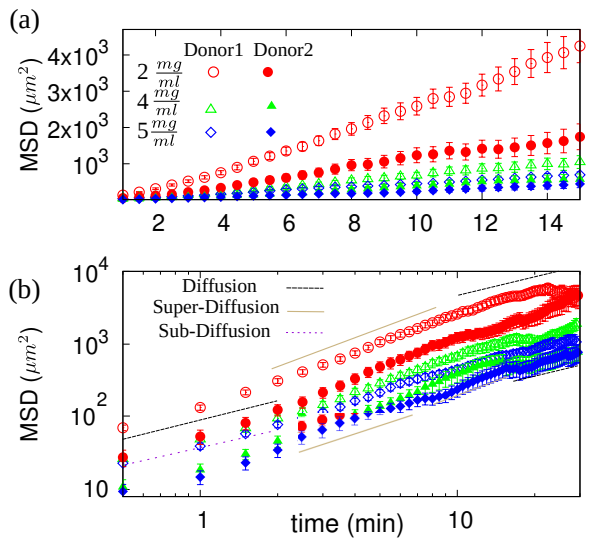

FIG. 3. Mean square displacement of CTLs in collagen matrices with different concentrations in (a) normal and (b) log-log scales.

The mean square displacements of different types of motion are clearly distinguishable (see e.g. Fig. 5(c)), indicating underlying differences between the dynamics of the three categories of motility.

B. The two-state motility type

Intermittent motion is widely observed in nature and it is shown that transitions between different internal states can help to optimize the search time [30]. In the following we study the mixed-velocity trajectories of T cells in more details.

Mean square displacement. The MSD of the mixed category coincides roughly with the total MSD, nearly in all cases (see the solid line in Fig. 5(c) for one sample). This indicates that the frequency of fast or slow periods in the mixed case have similar statistics as the purely fast or slow types of motion. In the next section, we compare

TABLE II. Percentage of different motility types of CTLs in collagen matrices with different densities.

	Donor 1			Donor 2		
density ($\frac{mg}{ml}$)	2	4	5	2	4	5
slow %	33	43	48	15	27	26
fast %	35	14	16	30	25	24
mixed %	26	37	25	48	40	43

the MSD of the mixed trajectories with the prediction of a two state random velocity model.

Exponential distribution of sojourn time in each state. The distribution of the times that the T cells remain in one state before they switch, the so-called sojourn times, follow an exponential decay as shown in figure 6. In this example the sojourn time distribution of T cells in the different states of the mixed T cell migration type of two donors in 4 mg/ml collagen concentration is plotted. The exponential decay of these distributions indicates that the transition probabilities are time-independent. This allows us to model the motion of T cells which switch to another motility state with a constant transition probability.

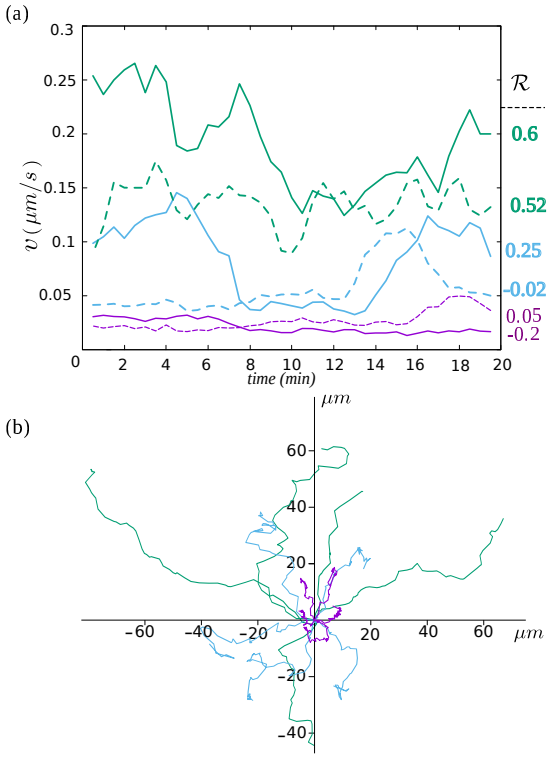

FIG. 4. (a) Typical velocities of CTL traces. Green, purple and blue colors correspond to fast, slow and mixed types of motility. (b) Typical trajectories of different motility types. The traces shown here are taken from Donor 1 in collagen with a concentration of 2 mg/ml.

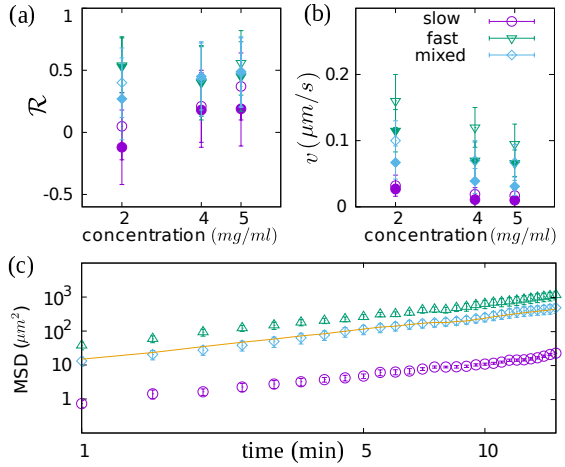

FIG. 5. (a) $\mathcal{R}$ and (b) velocity of different motility types in two donors represented by open and full symbols. (c) Mean square displacement of different motility types of donor 2 in collagen concentration 5 mg/ml. The solid line represents the MSD of all T cells.

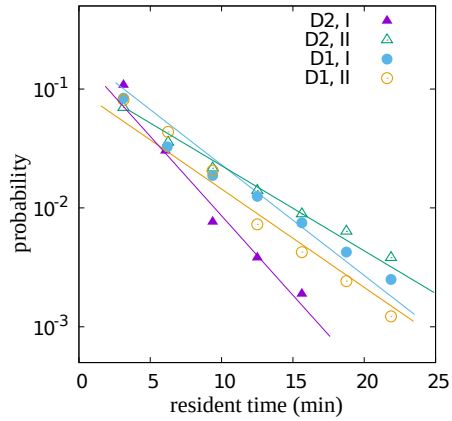

FIG. 6. Sojourn time distributions in the two states of mixed type of T cells in collagen with 4 mg/ml concentration. The lines are the corresponding theoretical estimate for each case (same color). D stands for donor.

IV. TWO-STATE PERSISTENT RANDOM WALK MODEL

In the following we show that the experimentally measured T cell trajectories are well described by a stochastic process that involves a persistent random walk with two different motility states [31]. We confine ourselves to a two-dimensional model to derive an analytical formula for the mean square displacement of one Cartesian coordinate $\langle x^2(t)\rangle$, which then multiplied by 3 to give the prediction for the MSD in three dimensions $\langle r^2(t)\rangle = 3\langle x^2(t)\rangle$[39].

We adopt a discrete-time approach, since it enables us to reproduce the detailed particle dynamics obtained from analyzing the experimental data. As the trajectories in experiments comprise a regularly recorded set of

particle positions, a continuous-time description fails to capture the short time behavior. By tracking the particle with a very fast camera, an extremely fine time resolution Δt compared to the characteristic time of particle wiggling can be obtained. In such a case, the consecutive orientations are correlated and the motion is supperdiffusive at short times with a crossover to normal diffusion at longer times. A discrete time formalism is able to capture such transient dynamics. Note that the initial dynamics in the limit $\Delta t \to 0$ is even a purely ballistic motion, thus, the discrete-time approach in this limit is inequivalent to the continuous-time description.

We consider persistent motions characterized by velocity distributions $F_{\rm I}(v)$ and $F_{\rm II}(v)$, and turning-angle distributions $R_{\rm I}(\phi)$ and $R_{\rm II}(\phi)$ for states I and II. We introduce the transition probabilities $\kappa_{\rm I\to II}$ and $\kappa_{\rm II\to I}$ for switching from state I to II and vice versa. These probabilities are estimated by the inverse of sojourn time in the two states of mixed trajectories, e.g. $\kappa_{\rm I\to II} \sim \langle\tau\rangle_{\rm I}^{-1}$. Constant probability transitions $\kappa_{\rm I\to II}$ ($\kappa_{\rm II\to I}$) lead to an exponential distribution of the sojourn time $\mathcal{F}_{\rm I}(\tau) \sim {\rm e}^{\ln(1-\kappa_{\rm I\to II})\,\tau}$ ($\mathcal{F}_{\rm II}(\tau) \sim {\rm e}^{\ln(1-\kappa_{\rm II\to I})\,\tau}$). As a first approximation, $\mathcal{F}_{\rm I}(\tau) \sim e^{-\tau/\langle\tau\rangle_I}$ and $\mathcal{F}_{\rm II}(\tau) \sim e^{-\tau/\langle\tau\rangle_{II}}$ are plotted in Fig. 6, which show a very good agreement with the experimental resident time distribution in each state of the mixed motion. Introducing the probability density functions $P_t^{\rm I}(x,y|\theta)$ and $P_t^{\rm II}(x,y|\theta)$ for the probability to find the walker at position (x,y) along the direction θ at time t in each of the motility states, the temporal evolution of the stochastic process can be described by the following set of coupled master equations:

$$\begin{aligned} P^{\rm I}_{t+\Delta t}(x,y|\theta) &= (1-\kappa_{\rm I\to II})\int dv F_{\rm I}(v)\int_{-\pi}^{\pi} d\gamma\, R_{\rm I}(\theta-\gamma) P_t^{\rm I}(x',y'|\gamma) \\ &\quad +\kappa_{\rm II\to I}\int dv F_{\rm I}(v)\int_{-\pi}^{\pi} d\gamma\, R_{\rm II}(\theta-\gamma)\, P_t^{\rm II}(x',y'|\gamma), \\ P^{\rm II}_{t+\Delta t}(x,y|\theta) &= (1-\kappa_{\rm II\to I})\int dv F_{\rm II}(v)\int_{-\pi}^{\pi} d\gamma\, R_{\rm II}(\theta-\gamma) P_t^{\rm II}(x',y'|\gamma) \\ &\quad +\kappa_{\rm I\to II}\int dv F_{\rm II}(v)\int_{-\pi}^{\pi} d\gamma\, R_{\rm I}(\theta-\gamma)\, P_t^{\rm I}(x',y'|\gamma), \end{aligned} \tag{1}$$

with $x' = x - v\Delta t\cos\theta$ and $y' = y - v\Delta t\sin\theta$. By solving these sets of master equations, one can evaluate arbitrary moments of the position of the walker, such as the mean square displacement. Several mathematical techniques like Fourier and z-transformation are used in order to solve equations 1. The z-transformation $A(z)$ of an arbitrary function A_n of a discrete variable $n = 0, 1, 2, ...$ is defined as $A(z) = \sum_{n=0}^{\infty} A_n z^{-n}$, which is equivalent to Laplace transformation in a continuous-time description. The exact result for the mean square displacement is obtained via inverse z transformation of [31]:

$$\begin{aligned} &\frac{1}{(\Delta t)^2}\sum_{t=0}^{\infty} z^{-t}\langle x^2\rangle(t) = \\ &\Big[\frac{z^2\kappa_{\rm II\to I}}{G_0(z)} + \frac{z(1-\kappa_{\rm II\to I}-\kappa_{\rm I\to II})P_0^{\rm I}}{z-1+\kappa_{\rm II\to I}+\kappa_{\rm I\to II}}\Big] \times \Big[\frac{z\left[z-(1-\kappa_{\rm II\to I})\mathcal{R}_{\rm II}\right]}{(z-1)G_1(z)}\langle v\rangle_{\rm I}^2 + \frac{z}{(z-1)G_1(z)}\kappa_{\rm I\to II}\mathcal{R}_{\rm II}\langle v\rangle_{\rm I}\langle v\rangle_{\rm II} - \frac{1}{z-1}\langle v\rangle_{\rm I}^2 + \frac{1}{2(z-1)}\langle v^2\rangle_{\rm I}\Big] \\ &+\Big[\frac{z^2\kappa_{\rm I\to II}}{G_0(z)} + \frac{z(1-\kappa_{\rm II\to I}-\kappa_{\rm I\to II})P_0^{\rm II}}{z-1+\kappa_{\rm II\to I}+\kappa_{\rm I\to II}}\Big] \times \Big[\frac{z\left[z-(1-\kappa_{\rm I\to II})\mathcal{R}_{\rm I}\right]}{(z-1)G_1(z)}\langle v\rangle_{\rm II}^2 + \frac{z}{(z-1)G_1(z)}\kappa_{\rm II\to I}\mathcal{R}_{\rm I}\langle v\rangle_{\rm II}\langle v\rangle_{\rm I} - \frac{1}{z-1}\langle v\rangle_{\rm II}^2 + \frac{1}{2(z-1)}\langle v^2\rangle_{\rm II}\Big], \end{aligned} \tag{2}$$

with

$$G_0(z) = (z-1)(z-1+\kappa_{\rm II\to I}+\kappa_{\rm I\to II})$$

and

$$G_1(z) = \Big[z-(1-\kappa_{\rm II\to I})\mathcal{R}_{\rm II}\Big]\Big[z-(1-\kappa_{\rm I\to II})\mathcal{R}_{\rm I}\Big] - \kappa_{\rm I\to II}\kappa_{\rm II\to I}\mathcal{R}_{\rm II}\mathcal{R}_{\rm I}$$

In equations 2, $\langle v\rangle_{\rm I}$, $\langle v\rangle_{\rm II}$, $\langle v^2\rangle_{\rm I}$ and $\langle v^2\rangle_{\rm II}$ are first and second moments of velocity of T cells in states I and II. $P_0^{\rm I} = 1 - P_0^{\rm II}$ is the initial condition and shows the probability of starting the motion in state I or equivalently the percentage of all T cells in state I at the beginning of tracking. $\mathcal{R}_{\rm I}$ and $\mathcal{R}_{\rm II}$ are the Fourier transform of distributions of turning angle $R_I(\phi)$ and $R_{II}(\phi)$ in Eqs.1:

$$\mathcal{R}_j = \int_{-\pi}^{\pi} {\rm d}\phi\, e^{i\phi} R_{\rm j}(\phi) = \langle cos\phi\rangle_j, j \in \{{\rm I}, {\rm II}\} \tag{3}$$

In the case of fast and slow types of motion, the master equations 1, shrinks to:

$$P_{t+\Delta t}(x,y|\theta) = \int dv F(v)\int_{-\pi}^{\pi} d\gamma\, R(\theta-\gamma) P_t(x',y'|\gamma). \tag{4}$$

Where $P_t(x,y|\theta)$ is the probability density of a T cell to arrive at position (x,y) with direction θ at time t and $F(v)$ and $R(\theta)$ are the distribution functions of velocity and turning angle, respectively. The resulting MSD in this case will be:

$$\begin{aligned} \langle x^2\rangle(t) &= (\frac{1}{2}\langle v^2\rangle + \frac{\mathcal{R}}{1-\mathcal{R}}\langle v\rangle^2)\Delta T t \\ &\quad + \frac{\mathcal{R}}{(1-\mathcal{R})^2}\langle v\rangle^2\Delta T^2(\mathcal{R}^{t/\Delta T} - 1) \end{aligned} \tag{5}$$

We do not use any fitting parameter, instead we extracted the model parameters from the experimental data

TABLE III. Parameters extracted from the experimental data of mixed type of motility and used in the two-state model.

	Donor 1			Donor 2		
density ($\frac{mg}{ml}$)	2	4	5	2	4	5
$V_I(\mu m/s)$	0.066	0.047	0.048	0.047	0.023	0.020
$V_{II}(\mu m/s)$	0.138	0.120	0.111	0.099	0.061	0.055
$V_I^2(\mu m^2/s^2)$	0.0189	0.0038	0.0037	0.0149	0.0009	0.0006
$V_{II}^2(\mu m^2/s^2)$	0.0510	0.0198	0.0165	0.038	0.0055	0.0040
R_I	0.15	0.35	0.38	0.19	0.26	0.35
R_{II}	0.62	0.59	0.59	0.33	0.56	0.69
Δt (min)	0.5	0.5	0.5	0.5	0.5	0.5
$\kappa_{\mathrm{I}\to\mathrm{II}}$	0.20	0.08	0.09	0.11	0.10	0.07
$\kappa_{\mathrm{II}\to\mathrm{I}}$	0.06	0.14	0.17	0.14	0.11	0.13

TABLE IV. Parameters extracted from the experimental data of fast (up) and slow(down) types of motility.

	Donor 1			Donor 2		
density ($\frac{mg}{ml}$)	2	4	5	2	4	5
$V_I(\mu m/s)$	0.17	0.12	0.09	0.11	0.07	0.07
$V_I^2(\mu m^2/s^2)$	0.033	0.019	0.013	0.018	0.008	0.006
R_I	0.54	0.41	0.45	0.53	0.40	0.56
Δt (min)	0.5	0.5	0.5	0.5	0.5	0.5
$V_I(\mu m/s)$	0.032	0.019	0.017	0.027	0.011	0.010
$V_I^2(\mu m^2/s^2)$	0.0014	0.0006	0.0005	0.0010	0.0002	0.0001
R_I	-0.12	0.18	0.19	0.05	0.21	0.37
Δt (min)	0.5	0.5	0.5	0.5	0.5	0.5

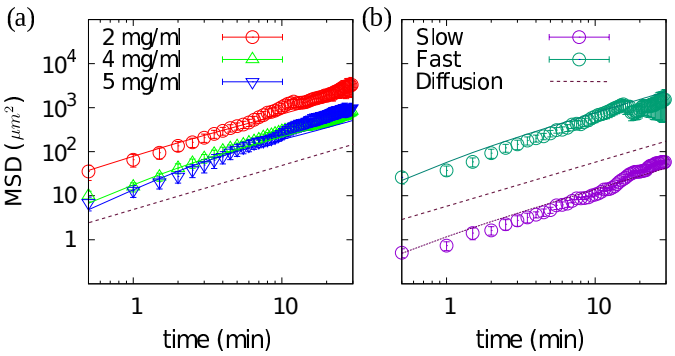

FIG. 7. (a) The mean square displacement of mixed motility type in various collagen concentrations obtained from the experiments (symbols) and analytical approach (Equation 2 with parameters extracted from experimental data summarized in table III) (solid lines) for donor 2. (b) The mean square displacement of slow and fast motility types in collagen concentration 4 mg/ml. The solid lines represent the theoretical estimate of equation6 withe parameters extracted from experiment (IV).

analysis. Moments of velocity ($\langle v\rangle_{\mathrm{I}}$, $\langle v\rangle_{\mathrm{II}}$, $\langle v^2\rangle_{\mathrm{I}}$ and $\langle v^2\rangle_{\mathrm{II}}$) in each state is calculated by averaging over local velocities of trajectories. The persistencies $\mathcal{R}_{\mathrm{I}}$ and $\mathcal{R}_{\mathrm{II}}$ are measured by averaging over *cosines* of turning angles (see Eq.3). The transition probabilities $\kappa_{\mathrm{I}\to\mathrm{II}}$ and $\kappa_{\mathrm{II}\to\mathrm{I}}$ are the inverse of average sojourn time in states I and II, respectively. The initial condition P_0^{I}, only affects the short-time behavior of motion, We set this parameter to 0 for all cases. This means that we assume all T cells start their motion in the faster mode. All extracted model parameters are summarized in Tables III and IV for mixed state and fast/slow states, respectively.

The time evolution of mean square displacement is shown in Fig. 7 for donor 2. Fig. 7 shows exemplary match of the model with the data. We emphasize that no fitting has been made to capture this agreement.

V. DISCUSSION

We analyzed the trajectories of CTLs of two donors within 3D collagen matrices with different concentrations. We found three motility types in all experiments: slow, fast and mixed. Similar motility types have been reported for natural killer (NK) cells in hydrogel collagen with a concentration of 3 mg/ml in the presence of target cells [28]. The similarity of the characteristics of CTL and NK cell trajectories points towards a common mechanism for migration of both cell types through collagen networks.

A plausible scenario is that the cells which arrive first in the collagen network perform a persistent random walk unless they move into denser areas of the network, where they become slower, but eventually find a way to move again, which leads to two-state motility. When the cells move through the collagen network, they leave a channel by displacing or stretching collagen fibers. These channels facilitate the movement of other T cells, such that cells entering already existing channels move faster and tend to remain in the existing channel network. They do not switch to slow movement and thus establish the fast type. The slow cells mainly remain in one part of the network and only "wiggle" around and seem to be nearly immobile.

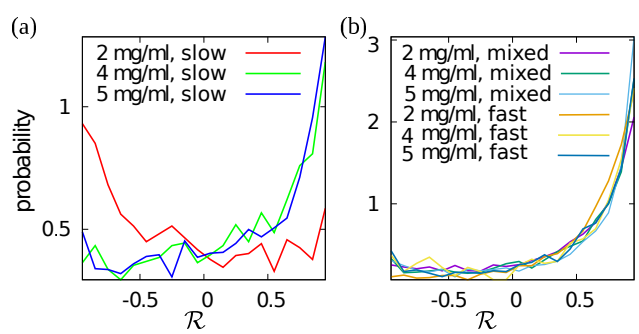

FIG. 8. Probability distributions of persistency $\mathcal{R}$ for different motility types in various concentrations of collagen, for (a) slow and (b) fast and mixed types.

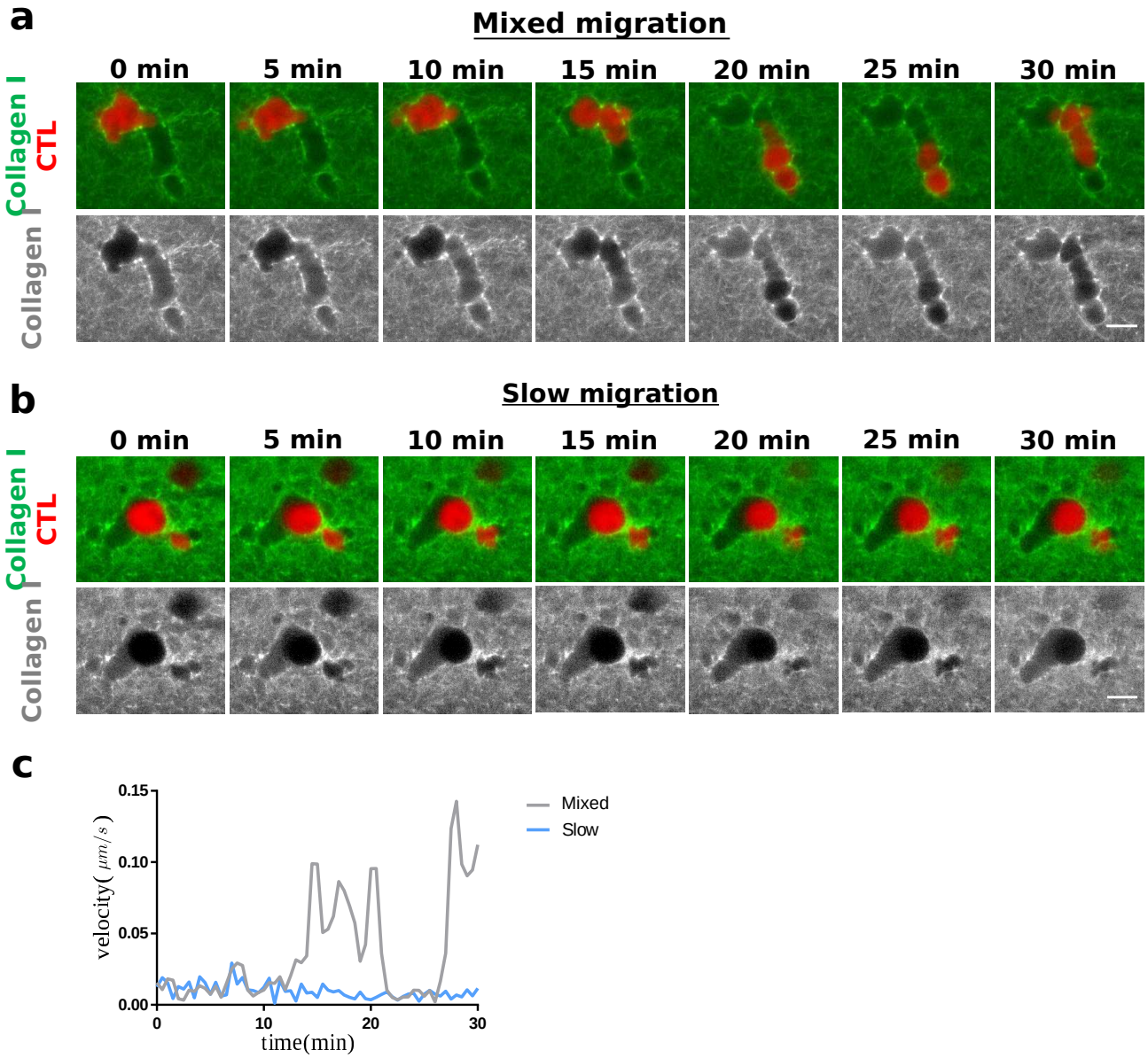

FIG. 9. Visualization of CTL migration in a collagen matrix. Primary Human CTLs were transiently transfected with mCherry (red). Collagen (5 mg/ml) was stained with Atto 488 NHS ester (green or gray as indicated). CTL migration was visualized at 37°C using lightsheet microscopy. Exemplary cells for mixed and slow migration are shown in a and b, respectively (Movies in Suppl. info). One layer of z-stack is presented. c, Quantification of migration velocity at all time points examined. CTL migration trajectories were tracked and analyzed by Imaris. Scale bars are 10 μm.

By studying the motion in different collagen densities, we found that the collagen concentration dependence of the persistency of slow T cells is different from the other types. Figure 8 shows the probability distribution of persistencies of the three different cell types. While the distributions for fast and mixed types show a persistent motion in all concentrations, slow T cells perform anti-persistent motion in 2 mg/ml collagen and become persistent in denser ones. We propose three explanations for these observations: 1) The slow cells have an activity level that is below that of the mixed and fast type, for instance due to an incomplete activation. 2) The slow T cells entered accidentally a region of the collagen matrix where still no channels produced by other T cells (within the 2 hours initiation time before measurements) and can only move forward by creating a new channel by deforming and/or destroying the collagen fibers, which is slow process as compared to fast migration with a channel. 3) The fast/mixed T cells and the slow T cells establish two different phenotypes. To test Explanation number 2, we fluorescently stained collagen and visualized the movements of CTLs using lightsheet microscopy. We found that during migration, CTLs could enter channels in collagen matrix. Inside the

channel they had high speed and when leaving the channel significantly slowed them down (Fig. 9a, 9c (Suppl. Movie 1)). Slow CTLs appeared to be trapped in some channels and the corresponding speed stayed slow (Fig. 9b, 9c (Suppl. Movie 2)). These results support the Explanation 2. Still, Explanations 1 and 3 should not be excluded. The morphology of the "channel" visible in Fig. 9 is incompatible with a randomly generated filament network (see background). The latter has of course randomly distributed regions with higher and lower filament density but elongated cylindrical tunnels as visible in Fig. 9 with a diameter of approximately equal to the diameter of a T cell and completely void of filaments cannot occur with significant probability by chance. These cylindrical tunnels are also unlikely to be produced by deformation: collagen fibers are elastic and will at least partially spring back once T cell has passed. More plausible appears to us the hypothesis that these channels have been produced by either T cells degrading the local matrix by secretion of matrix metalloproteases or by T cells tearing matrix apart by exertion of mechanical forces during the 2 hours before the observation and tracking was started - and leaving behind elongated, cylindrical tunnels of approximately the same diameter as T cells. Concerning the former option, it is reported that treatment of MMP inhibitor in human CD4 T-blast does not affect T cell speed [40](Fig. 5D). In $CD4^+$ T cells, MMP2 and MMP9 is expressed [41] , which do not degrade collagen type I [42], the type we used in our model. The collagen type I-degrading MMPs (MMP1, MMP8, MMP12 and MMP14) are not expressed in bead-stimulated primary human $CD8^+$ T cells [43]. Due to lack of MMPs, channel formation most probably proceeds via collagen filament deformation or destruction rather than degradation. It would be rewarding to catch a T cell in the act of deforming the local matrix and analyse it with time lapse microscopy - but we have to leave this endeavor for future experiments.

ACKNOWLEDGEMENTS

We acknowledge financial support from Collaborative Research Center SFB 1027, M.H. from BMBF grant 031L0133 and R.Z. from HOMFOR2018 grant.

[1] Zhang, N. and M. J. Bevan, "CD8(+) T cells: foot soldiers of the immune system." Immunity 35(2): 161 (2011)

[2] Krummel, M. F., F. Bartumeus, and A. Gerard, 2016.T cell migration, search strategies and mechanisms. Nat Rev Immunol 16(3): 193.

[3] Fearnley, D. B., L. F. Whyte, S. A. Carnoutsos, A. H. Cook, and D. N. Hart, 1999.Human blood dendritic cell numbers in normal individuals and in stem cell transplantation. Blood 93:728.

[4] Fricke, G. M., K. A. Letendre, M. E. Moses, and J. L. Cannon, 2016.Persistence and Adaptation in Immunity: T Cells Balance the Extent and Thoroughness of Search. PLoS Comput. Biol. 12: 3.

[5] Baumgart, F., M. Schneider, and G. J. Schütz,2019.How T Cells Do the 'Search for the Needle in the Haystack'. Front. Phys. 7:11.

[6] Moses, M. E., J. L. Cannon, D. M. Gordon, and S. Forrest, 2019. Distributed Adaptive Search in T Cells: Lessons From Ants. Front. Immunol. 10:1357.

[7] Bajenoff, M., et al., 2006. Stromal cell networks regulate lymphocyte entry, migration, and territoriality in lymph nodes. Immunity 25(6): 989.

[8] Beauchemin, C., N. M. Dixit, and A. S. Perelson, 2007. Characterizing T cell movement within lymph nodes in the absence of antigen. J. Immunol. 178: 5505.

[9] Preston, S. P., et al., 2006. T cell motility in the early stages of the immune response modeled as a random walk amongst targets. Phys. Rev. E Stat. Nonlin. Soft Matter Phys. 74, 011910.

[10] Miller, M. J., S. H. Wei, I. Parker, and M. D. Cahalan, 2002. Two-photon imaging of lymphocyte motility and antigen response in intact lymph node. Science 296(5574): 1869-1873.

[11] Crapo, P. M., T. W. Gilbert, and S. F. Badylak, 2011. An overview of tissue and whole organ decellularization processes. Biomaterials 32(12): 3233.

[12] Harris, T. H., et al., 2012. Generalized Levy walks and the role of chemokines in migration of effector CD8+ T cells. Nature 486(7404): 545.

[13] Applegate, K. G., C. M. Balch, and N. R. Pellis, 1990. In Vitro Migration of Lymphocytes through Collagen Matrix: Arrested Locomotion in Tumor-infiltrating Lymphocytes. CANCER RESEARCH 50: 7153.

[14] Rygiel, T. P., E. H. Stolte, T. Ruiter, M. L. van de Weijer, and L. Meyaard, 2011. Tumor-expressed collagens can modulate immune cell function through the inhibitory collagen receptor LAIR-1. Molecular Immunology 49: 402.

[15] Xu. S., et al., 2019. The role of collagen in cancer: from bench to bedside. J. Transl. Med.17:309.

[16] Zhou. Z. H., et al., 2017. Reorganized Collagen in the Tumor Microenvironment of Gastric Cancer and Its Association with Prognosis. J. Cancer 8:8.

[17] Han. W., et al., 2016. Oriented collagen fibers direct tumor cell intravasation. Proc. Natl. Acad. Sci. 113 (40) 11208.

[18] Miyazaki. K., et al., 2019. Cancer cell migration on elongate protrusions of fibroblasts in collagen matrix. Sci. Rep. 9:292.

[19] Provenzano, P. P., et al., 2006. Collagen reorganization at the tumor-stromal interface facilitates local invasion. BMC Med. 4(1):38.

[20] Lu, P., V. M. Weaver, and Z. Werb, 2012. "The extracellular matrix: A dynamic niche in cancer progression." J. Cell Biol. 196 (4): 395.

[21] Kuczek. D. E., et al., 2018. Collagen density regulates the activity of tumor-infiltrating T cells. bioRxiv. doi 10.1101/493437.

[22] Eyileten, C., et al., 2016. Immune Cells in Cancer Therapy and Drug Delivery. Mediators of inflammation vol.

2016:5230219.

[23] Xie, Z., et al., 2017. Immune Cell-Mediated Biodegradable Theranostic Nanoparticles for Melanoma Targeting and Drug Delivery. Small 13: 1603121.

[24] Haston, W. S., J. M.Shields, and P. C. Wilkinson, 1982. Lymphocyte locomotion and attachment on two-dimensional surfaces and in three-dimensional matrices. J. Cell Biol. 92:747.

[25] Schor, S. L., T. D. Allen, and B. Winn, 1983. Lymphocyte migration into three-dimensional collagen matrices: a quantitative study. J. Cell Biol. 96:1089.

[26] Friedl, P., E. B. Bröcker, and K. S. Zänker,1998. Integrins, cell matrix interactions and cell migration strategies: fundamental differences in leukocytes and tumor cells. Cell Adhes.Commun. 6:225.

[27] Artym, V. V., and K. Matsumoto, 2010. Imaging cells in three-dimensional collagen matrix. Curr Protoc Cell Biol, 10: p. Unit 10 18 1-20.

[28] Olofsson, P. E., et al., 2019. A collagen-based microwell migration assay to study NK-target cell interactions. Sci Rep 9, 10672.

[29] Pruitt, H. C., et al., 2019. Collagen fiber structure guides 3D motility of cytotoxic T lymphocytes. MATBIO-1550, 13.

[30] Bénichou, O., C. Loverdo, M. Moreau, and R. Voituriez, 2011. Intermittent search strategies. Rev Mod Phys 83:81.

[31] Shaebani, M. R., and Z. Sadjadi, 2019. Correlations and Memory Effects in Active Processes with Distinct Motility States. submitted (arXiv:1909.05033).

[32] Kummerow, C., et al., 2014. A simple, economic, time-resolved killing assay. Eur. J. Immunol. 44: 1870.

[33] Kanda, T., K. F. Sullivan, and G. M. Wahl, 1998. Histone-GFP fusion protein enables sensitive analysis of chromosome dynamics in living mammalian cells. Curr Biol. 8(7):377.

[34] Schoppmeyer, R. et al., 2017. Human profilin 1 is a negative regulator of CTL mediated cell-killing and migration. Eur. J. Immunol. 47: 1562.

[35] Schoppmeyer, R., R. Zhao, M. Hoth, and B. Qu, 2018. Light-sheet Microscopy for Three-dimensional Visualization of Human Immune Cells. J. Vis. Exp. 136:57651.

[36] Cox, T. R. and C. D. Madsen, 2017. Relative Stiffness Measurements of Cell-embedded Hydrogels by Shear Rheology in vitro. ďżźBio-protocol 7(1): e2101.

[37] Ayyildiz, M., S. Cinoglu, C. Basdogan, 2015. Effect of normal compression on the shear modulus of soft tissue in rheological measurements. J. Mech. Behav. Biomed. Mater 49:235.

[38] Wang, Y., M. F. Insana, 2013. Viscoelastic properties of rodent mammary tumors using ultrasonic shear-wave imaging. Ultrason. Imaging 35(2):126.

[39] Sadjadi, Z., M. R. Shaebani, H. Rieger, and L. Santen, 2015. Persistent-random-walk approach to anomalous transport of self-propelled particles. Phys. Rev. E 91:062715.

[40] Wolf, K., M. Lindert, M. Krause, S. Alexander, J. Riet, A. L. Willis, R. M. Hoffman, C. G. Figdor, S. J. Weiss and P. Friedl, 2013. Physical limits of cell migration: Control by ECM space and nuclear deformation and tuning by proteolysis and traction force. J Cell Biol. 201 (7): 1069.

[41] Edsparr, K., P. H. Basse, R. H. Goldfarb, and P. Albertsson, 2011. Matrix Metalloproteinases in Cytotoxic Lymphocytes Impact on Tumour Infiltration and Immunomodulation Cancer Microenviron. 4(3): 351.

[42] Jablonska-Trypuc, A., M. Matejczyk and S. Rosochacki,2016. Matrix metalloproteinases (MMPs), the main extracellular matrix (ECM) enzymes in collagen degradation, as a target for anticancer drugs. J. Enzyme Inhib. Med. Chem. 31 (sup1):177.

[43] E. Schwarz et al, to be published.